Induced Microcracking Affects Osteoblast Attachment on Hydroxyapatite Scaffolds for Tissue Engineering

Ian O. Smith, Melissa J. Baumann, Eldon D. Case
Department of Chemical Engineering and Materials Science, Michigan State University,
East Lansing, Michigan, 48824

Abstract: Bone microdamage caused by routine activity plays an important role in triggering targeted and nontargeted bone remodeling. Targeted remodeling occurs near localized areas of microdamage[1-4]. We hypothesize that bone remodeling may be directly and positively influenced by inducing microcracks in hydroxyapatite (HA) scaffolds for bone tissue engineering. A study by Case et al. showed microcracking in HA discs having >98% theoretical density[5]. These microcracks occurred without the application of external stress, likely as a result of thermal expansion anisotropy (TEA). TEA generates microcracks only when the specimen grain size exceeds a critical value (G_{CR}). Due to conflicting data in the literature on the thermal expansion along the crystallographic axes of HA, it is difficult to estimate G_{CR} precisely for HA, but G_{CR} likely ranges from a few tenths of microns to several microns[6]. As the grain size of a polycrystalline specimen increases above the critical grain size, the number of microcracks also increases but the number density of microcracks is difficult to control. Therefore, in this study we used Vickers microindentation to induce controlled microcracks in >99% dense HA discs. The effect of microcracking on the osteoblast (OB) attachment was then quantified. Control HA discs and microcracked HA were seeded with MC3T3-E1 OBs and cultured for 4 hours. The OBs were then stained with Rhodamine-Phalloidin and Hoechst fluorescent dyes to identify the actin fibers and nuclei, respectively. OB attachment was quantified using fluorescent light microscopy. OB attachment at 4 hours was 29% ± 7.6% of the initial seeded OBs for the microcracked HA specimens and 18% ± 6.1% of initial seeded OBs for the non-microcracked control HA specimens. The difference in these OB attachment values was statistically significant as determined via the Student t-test ($p = 0.004$, with $p < 0.05$ taken to indicate significance).

Key words: microcracking, hydroxyapatite, osteoblast attachment, ceramic, scaffold

INTRODUCTION

Microcracking in Bone

In a 1960 study of cracks located primarily in the cement line of human rib bones, Frost[7] first suggested that microcracking in bone results from mechanical fatigue. These cracks were not exclusively an artifact of specimen preparation, but rather an inherent characteristic of the bone. More recently, similar cracks have been observed in human[8-10], bovine[10, 11], canine[1, 12] and equine bone[13, 14]. Zioupos et al. report the size of these cracks as 10 – 50 μm in length with an apparent opening of 2 – 5 μm[11].

Bone exposed to routine activity undergoes repeated cyclic strain, on the order of 0.0003 to 0.0008 and 0.0008 to 0.0012 for walking and running, respectively[15, 16]. While these values are lower than the maximum strain allowed by bone in a single cycle, their repetitive nature leads to an accumulation of microcracks[17]. Left unchecked, this microdamage coalesces into macrocracks that can cause failure of the bone[8, 18, 19]. The process of microcrack accumulation to produce macrocracks is especially pronounced in aged individuals[9]. Frost also suggested a relationship between bone microcracking and subsequent bone remodeling[7]. Microdamage in bone likely triggers both targeted and nontargeted remodeling[20]. Nontargeted remodeling is not site dependant and occurs less frequently[21], while targeted remodeling occurs at sites of localized microdamage as observed in studies by Johnson et al., Burr et al. and Mori et al[2-4, 13]. In these cases, remodeling was significantly more focused around regions of microdamage[22]. Remodeling occurs when osteoclasts resorb damaged bone, including osteocytes[22]. The resorption process is regulated by the osteocyte syncytium in local regions of remodeling[23-25]. Osteocyte damage and subsequent apoptosis leads to increased osteoclast activity followed by subsequent osteoblast activity. Because microcracks occur with routine fatigue loading, the dynamic repair of microdamage is therefore an integral part of maintaining the integrity of the bone[2].

Microcracking in Hydroxyapatite

Case et al. were the first to definitively identify microcracking in dense (>98% theoretical density) HA

Corresponding Author: Prof. Melissa J. Baumann, Department of Chemical Engineering and Materials Science, Michigan State University, East Lansing, Michigan 48824

which occurred in the absence of an external applied stress[5]. This microcracking was likely a result of thermal expansion anisotropy (TEA), since non-cubic crystalline materials such as HA have dissimilar thermal expansion coefficients along the crystallographic axes. As a polycrystalline body cools following sintering, TEA causes neighboring grains to shrink at differing rates and in turn generates a stress that is sufficient to cause microcracking if the mean grain size exceeds a critical grain size, G_{CR}. Although TEA generated microcracks were observed in the dense HA specimens (average grain size of 7.9 μm ± 1.5 μm) examined by Case et al.[5], it is difficult to precisely estimate G_{CR} for HA. As discussed by Hoepfner et al., there are large disparities among the values reported in the literature for the thermal expansion coefficient as a function of crystallographic direction, which lead to large uncertainties in calculating G_{CR} for HA[6].

In general, the number density of microcracks increases with increasing grain size, but in the absence of extensive measurements, it is difficult to precisely predict changes in TEA-induced microcracks. Furthermore, there is no control over the spatial distribution of TEA-induced microcracks. Therefore in our HA specimens, in order to control both the number density and placement, microcracks were induced by Vickers micro-indentation where the microcrack length was controlled by varying the indentation load. The following relationships were used to predict the microcrack length (2c) and the indentation impression diagonal length (2a)

$$K_C = \alpha \left(\frac{E}{H} \right)^{\frac{1}{2}} \left(\frac{P}{C^{\frac{3}{2}}} \right) \qquad (1)$$

$$H = 1.8544 \left(\frac{P}{2a^2} \right) \qquad (2)$$

where K_C is fracture toughness, E is elastic modulus, H is hardness, P is indentation load, and α is a calibration constant, using values of K_C = 1 MPa√m, E = 115 GPa and α = 0.016[26, 27].

The array of Vickers indentations resulted in an areal distribution of microcracks. Cell counting was used to quantify OB attachment on both the microcracked and the nonmicrocracked HA specimens. The effect of microcracking on OB morphology was assessed by direct observation using optical fluorescence microscopy. A spindle shaped or polygonal spread OB morphology was then used as an indicator of typical OB attachment to the HA specimen surfaces[28-31].

MATERIALS AND METHODS

Powder processing

Dense HA discs were fabricated using high purity powder (Taihei Chemical, Osaka, JP) with a vendor-specified mean particle size of 1 - 3 μm. In a binderless process developed by McMullen, HA powder was uniaxially pressed into discs at 35 MPa for 1 minute using a KBr pellet die (International Crystal Laboratories, Garfield, NJ) or a hydraulic press (Carver Inc, Wabash, IN)[32]. The resulting HA powder discs (diameter = 32 mm, thickness = 2 – 3 mm) were sintered in air at 1360°C for 4 hours, at a heating/cooling rate of ~10°C/minute resulting in HA discs of 23 mm in diameter and 1 - 2 mm in thickness and >99% theoretical density as determined by Archimedes method (n = 5). The sintered HA specimen grain size was 4.8 μm ± 1.0 μm, determined by the line-intercept method (n = 5).

The surfaces of the HA discs were ground flat using 30 μm (600 grit) SiC wet abrasive paper and then all were sequentially polished using 30 μm, 12 μm, 9 μm, 6 μm and 1 μm diamond abrasive suspension or paste for 5 minutes at each grade. A Buehler EcoMet 3 variable speed grinder/polisher and an AutoMet 2 power head were used to grind and polish. Polished specimens were ultrasonically cleaned by submersion in reverse osmosis (RO) water followed by pulsing with an ultrasonic probe at 20 kHz and 250 Watts for 5 minutes.

Microcrack Induction

Surface-breaking microcracks were induced by indenting each specimen 196 times using a Buehler Micromet II microindenter (Buehler, Lake Bluff, IL), with a load of 4.9 N, a load time of 5 seconds and a loading rate of 70 μm/sec. These loading parameters were found by the authors to be the optimum set of conditions for inducing microcracks with minimal spalling and chipping of the HA specimens.

Indentations were made over a single 14 mm x 14 mm grid, with a one mm indentation spacing, across each specimen surface. The square-based pyramidal diamond indenter tip used for Vickers indentations creates diamond-shaped impressions on the HA disc surface. Microcracks are formed by the radial cracks originating from the corners of these indentation impressions (See Figure 1, where white arrows indicate radial cracks). Following indentation, each HA disc was submerged in RO water for 8 hours to insure crack growth saturation. The average indentation size and crack size were determined by optical microscopy for a representative selection of indentations (n = 20) on each HA specimen. A preliminary study of the effect of HA specimen immersion in RO water was conducted, in which 8 indentations were applied to a single dense HA disc, which was submerged in RO water, to determine the effectiveness of this treatment in assisting crack

growth. Crack length was measured at t = 30 seconds immediately following indentation, as well as at submersion times of 8 and 24 hours. The results of this trial are mentioned in addition to the average indent size and post-saturation crack length in the results section.
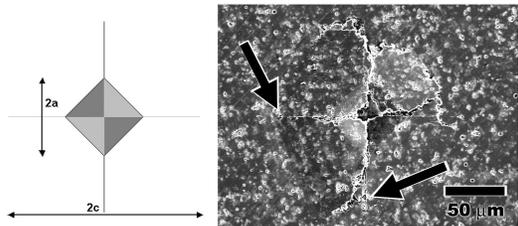

Fig. 1: SEM micrograph of microindentation on HA specimen surface (right). "2a" indicates the diagonal length of the indentation impression and "2c" indicates crack length (left).

MC3T3-E1 culture

MC3T3-E1 osteoblasts (OBs) of subclone 14, obtained from ATCC (Manassas, VA) were thawed and plated. The OBs were cultured using alpha minimum essential media (α-MEM, Invitrogen Grand Island, NY) supplemented with 10% fetal bovine serum (FBS, Atlanta Biologicals, Lawrenceville, GA), incubated in a humid atmosphere at 37°C and 5% CO_2. The OBs were split regularly with cell passages 25-29 used for this study.

OB attachment study

Microcracked HA and control HA disc specimens were autoclave sterilized, collared and placed into 6-well polystyrene cell culture plates in preparation for OB seeding. Prior to seeding, OBs were removed by trypsinization (Trypsin/EDTA, Invitrogen, Grand Island, NY), counted with a hemacytometer, centrifuged and resuspended in fresh complete α-MEM. Following standard procedures, OBs were seeded onto the HA discs at a density of 11,320 cells/cm^2 and enough media was added to account for evaporation[33]. After 4 hours incubation at 37°C and 5% CO_2 in a humid environment, the media was removed and each HA specimen washed using 1X phosphate buffered saline (PBS), to remove any non-attached OBs. OB seeding was done in triplicate, with n = 3 for a total of nine microcracked HA and nine control HA specimens.

OBs were fixed using 3.7% formaldehyde (H_2CO) (JT Baker, Phillipsburg, NJ) and permealized with a solution of 0.1% Triton X-100 (Sigma-Aldrich, St. Louis, MO). Prior to staining, OB seeded HA specimens were pre-incubated in 1% bovine serum

albumin (BSA, Invitrogen).

The actin cytoskeleton was stained using Rhodamine-Phalloidin while the nucleus was stained using Hoechst 33342 stain (Invitrogen)[32]. Stained OB seeded HA specimens were mounted in glycerol solution (JT Baker) and viewed using a Leica DM IL fluorescence microscope (Leica Microsystems, Wetzlar, GER) and optical micrographs recorded using the Spot RT camera (Diagnostic Instruments, Inc., Sterling Heights, MI). Rhodamine-Phalloidin stain fluoresces at a wavelength of $\lambda_{emmision}$ = 565 nm when exposed to light of wavelength $\lambda_{excitation}$ = 542 nm while the Hoechst stain fluoresces at a wavelength of $\lambda_{emmision}$ = 465 nm when exposed to light with wavelength of $\lambda_{excitation}$ = 355 nm.

OB attachment was quantified by counting nuclei over the microscope's field of view. Ten fields of view were randomly selected and counted for each specimen. The student's t-test was used to determine statistical significance, with $p < 0.05$ taken as significant.
The effect of induced microcracking in HA specimens on OB morphology was assessed by staining the actin fibers and observing the OB shape using optical fluorescence microscopy.

RESULTS AND DISCUSSION

Vickers indentation impressions in the dense HA specimens had an average diagonal length $2a_{AVE}$ = 54.7 μm ± 3.6 μm (Fig. 1). After crack saturation, the mean crack length was $2c_{AVE}$ = 176.3 μm ± 23.8 μm (Fig. 1).

Immersing microcracked HA specimens in RO water resulted in an increase in crack length from 143 μm ± 23.8 μm to 158 μm ± 17.4 μm after 8 hours and to 167 μm ± 14.0 μm after 24 hours (n = 8). This is consistent with previous findings that H_2O assists crack growth[34]. Student t-test determined that the increase in microcrack length between 8 and 24 hours was not significant.

Figure 2 is a plot of OB attachment at four hours for microcracked HA specimens (n = 9) and control HA specimens with no microcracking (n = 9), showing the significant difference in OB attachment between the two. Error bars indicate standard deviation. After 4 hours in culture, OB attachment on the microcracked HA specimens was 29% ± 7.6% of initial seeded OB number compared to 18% ± 6.1% of initial on the control HA specimens. This represents a 60% increase in OB attachment with microcracking. Student's t-test produced a p-value of 0.004, presence of microcracks on the HA surface had a positive and significant influence on OB attachment.
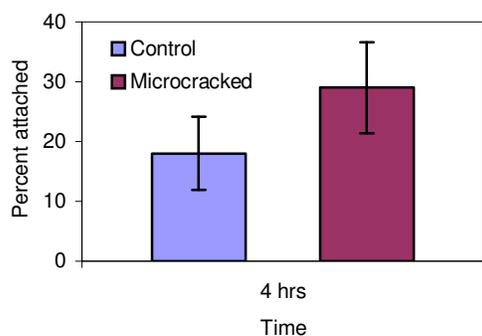
Fig. 2: Osteoblast attachment at 4 hours on microcracked and non-microcracked dense HA discs

The role of the Vickers indentations in increased OB attachment on HA specimens should be addressed. If we consider each indentation impression as a surface breaking pore of an average size $2a = 54.7$ μm ± 3.6 μm, then we can compare this size to that of typical pores designed to promote OB ingrowth. OBs respond to a bimodal system of pores, with pore sizes of 200 – 400 μm for macropores and < 70 μm for interconnecting micropores[35-37]. Since the Vickers indentation impressions do not approach this scale and do not include any interconnections, it is unlikely that they are the governing factor in increasing OB attachment.

Figure 3 includes optical micrographs showing OB attached to the surface of a control HA specimen (Fig. 3A) and OB attachment on a microcracked HA specimen (Fig. 3B). In addition to Hoechst stain to illuminate the cell nucleus, Rhodamine-Phalloidin stain was used to illuminate the actin fibers within the OBs The OBs attached to the surface of control HA have spread morphology (Fig. 3A), indicated by the either spindle-shaped or polygonal appearance of each cell. This spread morphology is consistent with the morphology of MC3T3-E1 OBs reported by Sudo et al. and others[28-31], and infers strong adhesion of the OBs to the HA substrate[38]. The presence of some spindle-shaped OBs and some polygonal OBs is consistent with observations of OB attachment on HA substrates at 4 hours by McMullen[39]. Figure 3B also shows the spread spindle-shaped morphology of the OBs on the surface of microcracked HA, indicating that the induction of microcracks on HA specimens does not change the shape of the attached OBs.
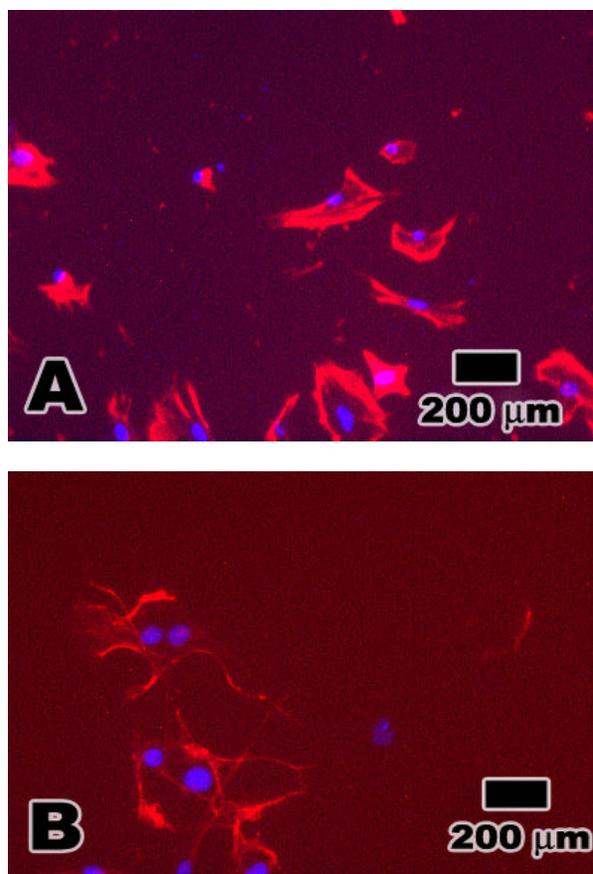

Fig. 3: 3A shows MC3T3-E1 osteoblasts with both spindle-shaped and polygonal morphology on HA control specimen, stained to highlight actin fibers (red – Rhodamine-Phalloidin) and nuclei (blue – Hoechst). 3B shows MC3T3-E1 Osteoblasts with spindle shaped morphology on HA microcracked specimen, stained to highlight actin fibers (red – Rhodamine-Phalloidin) and nuclei (blue – Hoechst).

CONCLUSION

Microcracked HA specimens showed 60% greater OB attachment *in* vitro compared to non-microcracked control HA specimens (Figure 2). To capture early attachment events, future studies to assess OB attachment at earlier times will be done. Additional studies are also needed to determine whether the induction of microcracks positively affects OB proliferation, differentiation and mineralization over time *in vitro*. However, the initial findings presented in this study indicate that microcracks enhance OB attachment activity. By mimicking the naturally occurring damage process that triggers bone remodeling, microcracks induced by Vickers indentation positively and significantly influenced the initial OB response to HA scaffolds.

REFERENCES

1. Johnson, K. A., Skinner, G. A. and Muir, P., 2001. Site-specific adaptive remodeling of Greyhound metacarpal cortical bone subjected to asymmetrical cyclic loading. Am J Vet Res, 62: 787-793.
2. Burr, D. B., Martin, R. B., Schaffler, M. B. and Radin, E. L., 1985. Bone remodeling in response to in vivo fatigue microdamage. J Biomech, 18: 189-200.
3. Burr, D. B. and Martin, R. B., 1993. Calculating the probability that microcracks initiate resorption spaces. J Biomech, 26: 613-616.
4. Mori, S. and Burr, D. B., 1993. Increased intracortical remodeling following fatigue microdamage. Bone, 14: 103-109.
5. Case, E. D., Smith, I. O. and Baumann, M. J., 2005. Microcracking and porosity in calcium phosphates and the implications for bone tissue engineering. Mat Sci and Eng A, 390: 246-254.
6. Hoepfner, T. P. and Case, E. D., 2004. An estimate of the critical grain size for microcracks induced hydroxyapatite by thermal expansion anisotropy. Mater Lett, 58: 489-492.
7. Frost, H. L., 1960. Presence of microscopic cracks in vivo in bone. Henry Ford Hospital Med Bull, 8: 27-35.
8. Blickenstaff, L. D. and Morris, J. M., 1966. Fatigue fracture of the femoral neck. J Bone Joint Surg, 48A: 1031-1047.
9. Schaffler, M. B., Choi, K. and Milgrom, C., 1995. Aging and matrix microdamage accumulation in human compact bone. Bone, 17: 521-525.
10. Lee, T. C., O'Brien, F. J. and Taylor, D., 2000. The nature of fatigue damage in bone. Int J Fatigue, 22: 847-853.
11. Zioupos, P. and Currey, J. D., 1994. The extent of microcracking and the morphology of microcracks in damaged bone. J Mat Sci, 29: 978-986.
12. Muir, P., Johnson, K. A. and Ruaux-Mason, C. P., 1999. In vivo matrix microdamage in a naturally occurring canine fatigue fracture. Bone, 25: 571-576.
13. Stepnik, M. W., Radtke, C. L., Scollay, M. C., Oshel, P. E., Albrecht, R. M., Santschi, E. M., Markel, M. D. and Muir, P., 2004. Scanning electron microscopic examination of third metacarpal/third metatarsal bone failure surfaces in thoroughbred racehorses with condylar fracture. Vet Surg, 33: 2-10.
14. Da Costa Gomez, T. M., Radtke, C. L., Kalscheur, V. L., Swain, C. A., Scollay, M. C., Edwards, R. B., Santschi, E. M., Markel, M. D. and Muir, P., 2004. Effect of focused and radial extracorporeal shock wave therapy on equine bone microdamage. Vet Surg, 33: 49-55.
15. Lanyon, L. E., Hampson, W. G. J., Goodship, A. E. and Shah, J. S., 1975. Bone deformation recorded in vivo from strain gauges attached to the human tibial shaft. Acta Orthop Scand, 46: 256-268.
16. Burr, D. B., Milgrom, C., Fyhrie, D. P., Forwood, M., Nyska, M., Finestone, A., Hoshaw, S., Saiag, E. and Simkin, A., 1996. In vivo measurement of human tibial strains during vigorous activity. Bone, 18: 405-410.
17. Park, J. B. and Lakes, R. S., 1992. Biomaterials: An Introduction. 2nd, Plenum Press, New York.
18. Schaffler, M. B., Radin, E. L. and Burr, D. B., 1989. Mechanical and morphological effects of strain rate on fatigue of compact bone. Bone, 10: 207-214.
19. Schaffler, M. B., Radin, E. L. and Burr, D. B., 1990. Long-term fatigue behavior of compact bone at low strain magnitude and rate. Bone, 11: 321-326.
20. Burr, D. B., 2002. Targeted and nontargeted remodeling. Bone, 30: 2-4.
21. Bentolila, V., Boyce, T. M., Fyhrie, D. P., Drumb, R., Skerry, T. M. and Schaffler, M. B., 1998. Intracortical remodeling in adult rat long bones after fatigue loading. Bone, 23: 275-281.
22. Bronckers, A. L. J. J., Goei, W., Luo, G., Karsenty, G., D'Souza, R. N., Lyaruu, D. M. and Burger, E. H., 1996. DNA fragmentation during bone formation in neonatal rodents assessed by transferase-mediated end labelling. J Bone Miner Res, 11: 1281-1291.
23. Colopy, S. A., Benz-Dean, J., Barrett, J. G., Sample, S. J., Lu, Y., Danova, N. A., Kalscheur, V. L., Vanderby Jr., R., Markel, M. D. and Muir, P., 2004. Response of osteocyte syncytium adjacent to and distant from linear microcracks during adaptation to cyclic fatigue loading. Bone, 35: 881-891.
24. Noble, B. S., Peet, N., Stevens, H. Y., Brabbs, A., Mosely, J. R., Reilly, G. C., Reeve, J., Skerry, T. M. and Lanyon, L. E., 2002. Mechanical loading: biphasic osteocyte survival and targeting of osteoclasts for bone destruction in rat cortical bone. Am J Physiol Cell Physiol, 284: 934-943.
25. Verborgt, O., Gibson, G. J. and Schaffler, M. B., 2000. Loss of osteocyte integrity in association with microdamage and bone remodeling after fatigue in vivo. J Bone Miner Res, 15: 60-67.
26. Wachtman, J. B., 1996. Mechanical Properties of Ceramics. 1, John Wiley and Sons, Inc., New York.
27. Suchanek, W., Yashima, M., Kakihana, M. and Yoshimura, M., 1996. Processing and mechanical properties of hydroxyapatite reinforced with hydroxyapatite whiskers. Biomaterials, 17: 1715-1723.

28. Du, C., Su, X. W., Cui, F. Z. and Zhu, X. D., 1998. Morphological behaviour of osteoblasts on diamond-like carbon coating and amorphous C-N film in organ culture. Biomaterials, 19: 651-658.

29. Puleo, D. A., Holleran, L. A., Doremus, R. H. and Bizios, R., 1991. Osteoblast response to orthopedic implant materials in vitro. J Biomed Mater Res, 25: 711-723.

30. Itakura, Y., Kosugi, A., Sudo, H., Yamamoto, S. and Kumegawa, M., 1988. Development of a new system for evaluating the biocompatibility of implant materials using an osteogenic cell line (MC3T3-E1). J Biomed Mater Res, 22: 613-622.

31. Sudo, H., Kodama, H. A., Amagai, Y., Yamamoto, S. and Kasai, S., 1983. In vitro differentiation and calcification in a new clonal osteogenic cell line derived from newborn mouse calvaria. J Cell Biol, 96: 191-198.

32. McMullen, R., 2004. An in vitro investigation of MC3T3-E1 osteoblast proliferation and differentiation on hydroxyapatite based tissue engineered scaffolds. Masters Degree Thesis, Michigan State University, page 43.

33. Shu, R., McMullen, R., Baumann, M. J. and McCabe, L. R., 2003. Hydroxyapatite accelerates differentiation and suppresses growth of MC3T3-E1 osteoblasts. J Biomed Mater Res, 67A: 1196-1204.

34. Case, E. D. and Kim, W. S., 1995. Comparison of thermal fatigue damage in unreinforced and reinforced alumina ceramics: crack lengths and macroscopic properties. 11th Annual Advanced Composites Conference, The Engineering Society, Ann Arbor, MI.

35. Flautre, B., Descamps, M., Delecourt, C. and Blary, M. C., 2001. Porous HA ceramic for bone replacement: role of the pores and interconnections - experimental study in rabbit. J Mat Sci: Mat Med, 12: 679-682.

36. Lu, J., Flautre, B., Anselme, K., Hardouin, P., Gallur, A., Descamps, M. and Thierry, B., 1999. Role of interconnections in porous bioceramics on bone recolonization in vitro and in vivo. J Mater Sci: Mater Med, 10: 111-120.

37. Yuan, H., Kurashina, K., deBruijn, J. D., Li, Y., deGroot, K. and Zhang, X., 1999. A preliminary study on osteoinduction of two kinds of calcium phosphate ceramics. Biomaterials, 20: 1799-1806.

38. Locci, P., Becchetti, E., Pugliese, M., Rossi, L., Belcastro, S., Calvitti, M., Pietrarelli, G. and Staffolani, N., 1997. Phenotype expression of human bone cells cultured on implant substrates. Cell Biochem Funct, 15: 163-170.

39. McMullen, R., 2004. An in vitro investigation of MC3T3-E1 osteoblast proliferation and differentiation on hydroxyapatite based tissue engineered scaffolds. Masters Degree Thesis, Michigan State University, page 119.